

UTIL: An Ultra-Wideband Time-Difference-of-Arrival Indoor Localization Dataset

The International Journal of Robotics Research
 XX(X):1–10
 ©The Author(s) 2022
 Reprints and permission:
 sagepub.co.uk/journalsPermissions.nav
 DOI: 10.1177/ToBeAssigned
 www.sagepub.com/



Wenda Zhao¹, Abhishek Goudar¹, Xinyuan Qiao¹, and Angela P. Schoellig¹

Abstract

Ultra-wideband (UWB) time-difference-of-arrival (TDOA)-based localization has recently emerged as a promising, low-cost, and scalable indoor localization solution, which is especially suited for multi-robot applications. However, there is a lack of public datasets to benchmark the emerging UWB TDOA positioning technology in cluttered indoor environments. To fill in this gap, we present a comprehensive dataset consisting of UWB TDOA identification experiments and flight experiments based on Decawave's DWM1000 UWB modules. In the identification experiments, we collected low-level signal information, including signal-to-noise ratio (SNR) and power difference values, in various line-of-sight (LOS) and non-line-of-sight (NLOS) conditions. For the flight experiments, we conducted a cumulative ~ 150 minutes of real-world flights with an average speed of 0.45 m/s using four different anchor constellations. Raw sensor data including UWB TDOA, inertial measurement unit (IMU), optical flow, time-of-flight (ToF) laser, and millimeter-accurate ground truth data were collected during the flights. The dataset and development kit are available at <https://utiasdsl.github.io/util-uwb-dataset/>.

Keywords

Ultra-wideband, time-difference-of-arrival, indoor localization

1 Introduction

Accurate and reliable indoor localization is a crucial enabling technology for many robotics applications, ranging from warehouse management to monitoring tasks. Over the last decade, ultra-wideband (UWB) radio technology has been shown to provide high-accuracy and obstacle-penetrating time-of-arrival (TOA) measurements that are robust to radio-frequency interference using tiny integrated circuits (Zafari et al. 2019). UWB chips have been integrated in the latest generation of consumer electronics like iOS and Android phones and smartwatches to support the spatially aware interactions (Apple 2022; Qorvo 2022; Robert Triggs 2022). In FIFA World Cup 2022, UWB-based localization technology is applied to an official football tournament, for the first time, to enhance the Video Assistant Referee (VAR) system by providing reliable, low-latency, and decimeter-level accurate ball tracking information (Adidas 2022; KINEXON 2022; Dowsett 2022).

Similar to the Global Positioning System (GPS) (Enge 1994), an UWB-based positioning system requires UWB radios (also called anchors) pre-installed with known positions in the environment as a constellation, which serve as landmarks for positioning. In autonomous robotics (Nguyen et al. 2021a; Pfeiffer et al. 2021), the two main ranging schemes used for UWB localization are (i) two-way ranging (TWR) and (ii) time-difference-of-arrival (TDOA). In TWR, the UWB module mounted on the robot (also called tag) communicates with an anchor and acquires range measurements through two-way communication. In TDOA, UWB tags compute the difference between the arrival times of the radio packets from two anchors as TDOA measurements.

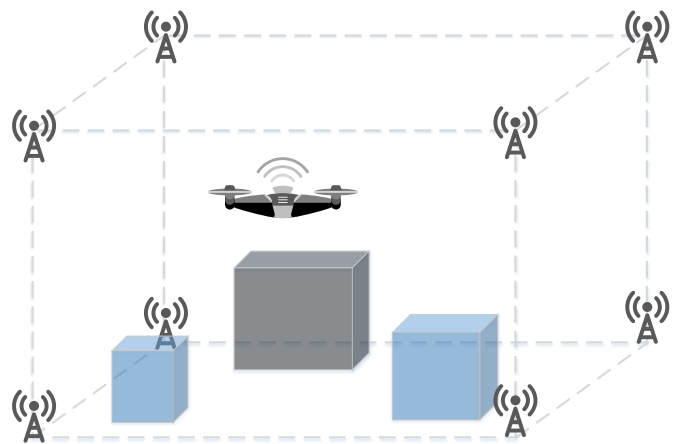


Figure 1. Sketch of an UWB TDOA localization system in a cluttered indoor environment. UWB anchors are pre-installed with known positions in the space. The robot, equipped with an UWB tag, receives TDOA measurements from the anchors for localization. Wooden and metal obstacles are used to create NLOS scenarios.

Compared with TWR, TDOA does not require active two-way communication between an anchor and a tag, thus enabling localization of a large number of devices (Hamer

¹Institute for Aerospace Studies, University of Toronto, Canada

Corresponding author:

Wenda Zhao, University of Toronto Institute for Aerospace Studies, Toronto, Ontario, M3H 5T6, Canada.
 Email: wenda.zhao@robotics.utias.utoronto.ca

and D'Andrea 2018). However, UWB TDOA-based localization systems still encounter difficulties in cluttered indoor environments. Delayed and degraded radio signals caused by non-line-of-sight (NLOS) and multi-path radio propagation can greatly deteriorate positioning accuracy. In order to achieve reliable UWB TDOA-based positioning in complex indoor environments, new algorithms are required to improve the localization accuracy and robustness.

To foster research in this domain, we present a comprehensive UWB TDOA dataset collected in a variety of cluttered indoor environments, including different types of static and dynamic obstacles. Low-cost DWM1000 UWB modules are used to construct cost-efficient indoor positioning systems for data collection. The dataset includes two parts: (i) an UWB TDOA identification dataset and (ii) a flight experiments dataset. In the identification dataset, we collected low-level UWB signal information such as signal-to-noise ratio (SNR) and power difference values in line-of-sight (LOS) and NLOS conditions to characterize UWB TDOA measurement performance. Obstacles of different types of materials commonly used in indoor settings, including cardboard, metal, wood, plastic, and foam, are used to create NLOS scenarios. For the flight dataset, we collected a cumulative ~ 150 minutes of real-world flight data with an average speed of 0.45 m/s using four different anchor constellations. Raw sensor data including UWB TDOA, inertial measurement unit (IMU), optical flow, time-of-flight (ToF) laser, and millimeter-accurate ground truth data from a motion capture system were collected during the flights.

The intended users of this dataset are researchers who are interested in UWB TDOA-based localization. The dataset can be used to model the UWB TDOA measurement errors under various LOS and NLOS conditions. Also, users can compare the UWB TDOA-based positioning performance (i) with different UWB anchor constellations, (ii) with and without obstacles, and (iii) with centralized and decentralized TDOA mode (introduced in Section 3). Further, the dataset users are encouraged to design new algorithms to enhance the accuracy and robustness of UWB TDOA-based positioning in cluttered indoor environments.

The main contributions of this dataset are as follows:

- An identification dataset for UWB TDOA measurements in a variety of LOS and NLOS scenarios involving obstacles with different type of materials, including plastic, wood, metal, etc.
- A comprehensive multi-modal dataset collected with a cumulative ~ 150 minutes of real-world flights in indoor environments cluttered with static and dynamic obstacles. We collected centralized and decentralized UWB TDOA measurements using four different anchor constellations for comparison.

2 Related Work

Many public UWB datasets have been produced in literature for a variety of applications, including UWB through-wall radar (Zhengliang et al. 2021), human motion tracking (Delamare et al. 2020; Vleugels et al. 2021), localization for mobile robots (Raza et al. 2019; Queralta et al. 2020; Nguyen et al. 2021b). Several UWB datasets accompanying research papers have also been made publicly

available (Barral et al. 2019a; Ledergerber and D'Andrea 2019; Pfeiffer et al. 2021). Considering the large amount of applications of UWB technology, we focus on UWB-based localization for mobile robots and summarize the related UWB datasets, to the best of our knowledge, in Table 1 for an overview.

From Table 1, we can observe that many of the public UWB datasets focus on UWB TWR-based localization. For UWB TDOA-based positioning, Raza et al. (Raza et al. 2019) provided a dataset to compare the performance of UWB TDOA and narrowband Bluetooth-based localization technologies. However, the dataset provides the data collected using only one anchor constellation in a simple indoor environment without obstacles. Pfeiffer et al. (Pfeiffer et al. 2021) released their dataset along with their research work including both UWB TWR and TDOA measurements collected from a Crazyflie 2.1 nano-quadrotor. However, the dataset is also created in an obstacle-free environment.

Realistic indoor environments often contain different types of obstacles which might interfere with UWB radio signals. In order to achieve accurate and reliable UWB TDOA-based indoor positioning, UWB measurements need to be tested in such scenarios. However, there exists an absence of UWB TDOA measurements identification and data collection in cluttered environment. Further, most of these datasets do not provide data collected in the presence of dynamic obstacles. We present an Ultra-wideband Time-difference-of-arrival Indoor Localization (UTIL) dataset to fill in this gap. In this dataset, we conducted extensive UWB TDOA identification experiments under LOS and NLOS scenarios and collected multi-modal sensor data from a quadrotor platform in the presence of static and dynamic obstacles. During the flight experiments, we collected raw UWB TDOA measurements with additional onboard sensor data (IMU, optical flow, and ToF laser) in four anchor constellations. Both centralized and decentralized TDOA measurements are collected under the same conditions for comparison. The combination of onboard sensors, different anchor constellations and TDOA modes, and diverse cluttered scenarios contained in this dataset enable detailed comparisons of UWB TDOA-based localization capabilities for quadrotors, which can not be done using existing datasets. To the best of our knowledge, a comprehensive UWB TDOA dataset with (i) identification experiments and (ii) data taken in a variety of indoor environments with static and dynamic obstacles does not exist in literature.

3 UWB TDOA-based Localization System

Our UWB TDOA-based localization system is sketched in Figure 1. Eight UWB anchors are pre-installed in the space with known positions. The robot equipped with an UWB tag computes the difference of the distances between the robot and the two transmitting anchors using the UWB signal arrival times. To better explain the content of our dataset, we introduce the UWB radio hardware used for data collection and provide a brief explanation of the TDOA principles.

3.1 UWB Sensor

We use the Decawave's DWM1000 (Decaware 2016) UWB radio sensors in this dataset. The DWM1000 module is a

Table 1. Public UWB dataset for mobile robot localization. The LOS/NLOS testing refers to experiments to identify and model UWB measurements under LOS/NLOS scenarios. Time Domain UWB modules are high-performance UWB radio sensors originally developed by Time Domain Corporation (TDSR 2022). Time Domain UWB modules can provide more accurate two-way ranging (TWR) measurements with a higher price compared to low-cost Decawave's DWM1000 modules.

Reference	UWB Mode	LOS/NLOS Testing	Anchor Constellations	Static Obstacle	Dynamic Obstacle	Dimension	UWB Module
(Li et al. 2018)	TWR	✗	1	✗	✗	3D	Time Domain
(Barral et al. 2019b)	TWR	✓	1	Obstacles with unkown material	✗	2D	DWM1000
(Arjmandi et al. 2020)	TWR	✗	5	✗	✗	3D	Time Domain
(Queralta et al. 2020)	TWR	✗	4	✗	✗	3D	DWM1001
(Nguyen et al. 2021b)	TWR	✗	3	✗	✗	3D	Time Domain
(Ledergerber and D'Andrea 2019)	TWR and CIR values	✓	4	Wood, metal, and fabric (chair)	✗	2D	DWM1000
(Pfeiffer et al. 2021)	TWR TDOA	✗	1	✗	✗	3D	DWM1000
(Raza et al. 2019)	TDOA	✗	1	✗	✗	2D	DWM1001
UTIL Dataset (ours)	TDOA	✓	4	Plastic, wood, metal, cardboard, and foam	Metal	3D	DWM1000

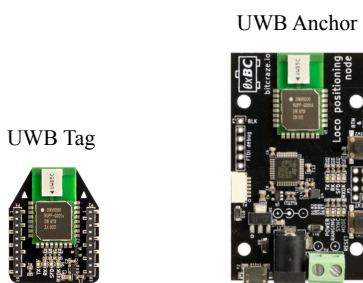


Figure 2. The Loco Positioning System (LPS) from Bitcraze, based on Decawave's DWM1000 UWB modules, is used for the data collection.

low-cost UWB radio often used to develop cost-efficient localization solutions. The Loco Positioning System (LPS) from Bitcraze (Bitcraze 2022b) based on DWM1000 UWB modules is used to collect UWB TDOA measurements.

Both centralized TDOA and decentralized TDOA (Meng et al. 2016) are implemented in LPS, which are referred to as TDOA 2 and TDOA 3 by Bitcraze, respectively. In centralized TDOA systems, all the anchors are synchronized w.r.t. one master anchor and the TDOA measurements are expressed in the same clock. However, centralized TDOA systems are limited by the communication constraints and suffer from single point failure (Ennasr et al. 2016). In decentralized TDOA systems, anchor pairs synchronize the timescales between each other and not with a single master anchor, which leads to scalability.

3.2 Time-difference-of-arrival Principles

In this subsection, we briefly explain the TDOA principles implemented in LPS. Without loss of generality, we denote a pair of UWB anchors as anchor 1 and anchor 2. The TDOA measurement d_{12} is the difference of distances of the tag to anchor 1 and 2. The sequence of the UWB radio packets among the anchor pair and one tag are visualized in Figure 3. UWB radios, both anchors and the tag, operate with their own clock, which are indicated as solid lines with different colors. A clock synchronization process is essential for an accurate computation of TDOA measurements.

We denote the clock of anchor 1, anchor 2, and the tag as cl_1 , cl_2 , and cl_T in the superscripts. The transmitting and

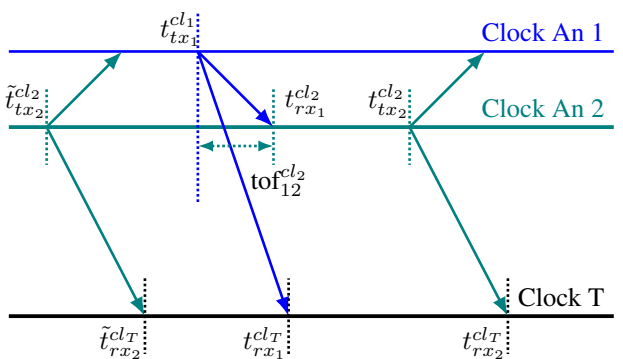


Figure 3. The sequence of UWB radio packets between the tag and anchor 1 and anchor 2. The clocks of anchor 1, anchor 2, and the tag are indicated as solid lines with different colors. The radio packets between the tag and anchors are denoted as solid arrow lines.



Figure 4. UWB anchors and tag setup for UWB identification experiments.

the receiving of a radio signal from anchor 1 are denoted as tx_1 and rx_1 in the subscripts. As an example, $t_{rx_2}^{cl_T}$ indicates the receiving timestamp of the radio packet from anchor 2 expressed in the tag's clock. UWB radio signals are transmitted with a scheduled transmission sequence. We use \tilde{t} to indicate the timestamp from the previous sequence: $\tilde{t}_{tx_2}^{cl_2}$ indicates the transmitting timestamp of the radio packet from anchor 2 expressed in the clock of anchor 2 from the previous sequence. With anchor 1 and anchor 2 at positions $\mathbf{a}_1, \mathbf{a}_2 \in \mathbb{R}^3$ and one tag at position $\mathbf{p} \in \mathbb{R}^3$, the TDOA measurement between anchor 1 and 2 is computed as

$$d_{12} = c \left[(t_{rx_2}^{cl_T} - t_{rx_1}^{cl_T}) - \alpha(t_{tx_2}^{cl_2} - \tilde{t}_{tx_2}^{cl_2} + \text{tof}_{12}^{cl_2}) \right], \quad (1)$$

$$= \|\mathbf{p} - \mathbf{a}_2\| - \|\mathbf{p} - \mathbf{a}_1\|$$

where c indicates the speed of light, α is the clock correction parameter converting from anchor 2's clock to the tag's clock, $\text{tof}_{12}^{cl_2}$ is the time-of-flight measurements between anchor 1 and anchor 2 expressed in anchor 2's clock, and $\|\cdot\|$ indicates the ℓ_2 norm. The clock correction parameter α is used to synchronize the clock of anchor 2 to the clock of the tag. We compute α with the timestamps from the previous sequence

$$\alpha = \frac{t_{rx_2}^{cl_T} - \tilde{t}_{rx_2}^{cl_T}}{t_{tx_2}^{cl_2} - \tilde{t}_{tx_2}^{cl_2}}. \quad (2)$$

4 Data Collection

4.1 Ground Truth

The UTIL dataset was produced in the University of Toronto Institute for Aerospace Studies (UTIAS). We collected the data in the indoor flight arena equipped with a motion capture system of 10 Vicon Vantage+ cameras (Vicon 2022). The millimeter-level accurate Vicon pose measurements were collected during UWB identification experiments and flight experiments as the ground truth measurements.

4.2 UWB Identification Dataset

In order to identify the UWB TDOA measurement performance in LOS and NLOS scenarios, we conducted a variety of LOS and NLOS experiments using two anchors

and one tag. Figure 4 demonstrates the experimental setup for the identification dataset. Two UWB anchors, referred to as anchor 1 and anchor 2, and one Crazyflie nano-quadrotor equipped with an UWB tag were placed on wooden structures. The ground truth pose data was provided by the motion capture system. Since only two anchors were used for the data collection, we ignored the difference between the centralized and decentralized TDOA modes and set the anchors into decentralized mode (TDOA 3). We collected the data through the Robot Operating System (ROS). Each sub-dataset was collected during a one-minute static experiment.

To assess the quality of received UWB signals, we collected the signal-to-noise ratio (SNR) and power difference (P_d) values provided in the Decawave user manual (Decawave 2017) as the performance metrics. The computation of SNR and power difference P_d are as follows

$$\text{SNR} = \frac{\text{Am}_f}{\sigma_n}, \quad P_d = P_r - P_f, \quad (3)$$

where Am_f indicates the *First Path Amplitude value*, σ_n indicates the *Standard Deviation of Channel Impulse Response Estimate Noise value*, and P_r and P_f are the total received power and the first path power, respectively. In general, a higher SNR value or a lower P_d indicates the received radio signal is of good quality (Decawave 2017). The four raw measurements $\{\text{Am}_f, \sigma_n, P_r, P_f\}$ can be accessed from the DW1000 UWB chip when receiving an UWB radio signal. We refer to Section 4.7 of the user manual (Decawave 2017) for more information. Detailed data format and descriptions of the UWB identification dataset are provided in Section 5.1.

4.2.1 Line-of-sight tests. We collected UWB TDOA measurements from two LOS identification tests: (i) the LOS distance test and (ii) the LOS angle test. The data collection procedures are sketched in Figure 5a-b. The positions of the tag and anchor 2 are fixed throughout the LOS data

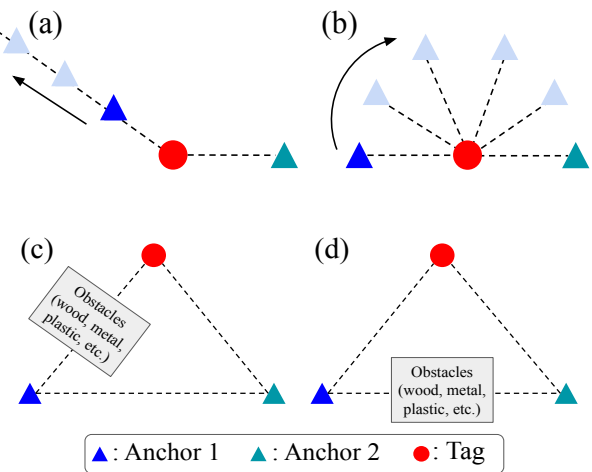


Figure 5. A diagram of the UWB identification experiments. The experiment process of LOS distance tests and LOS angle tests are illustrated in (a) and (b). The NLOS identification tests between an anchor and a tag and between two anchors are shown in (c) and (d).

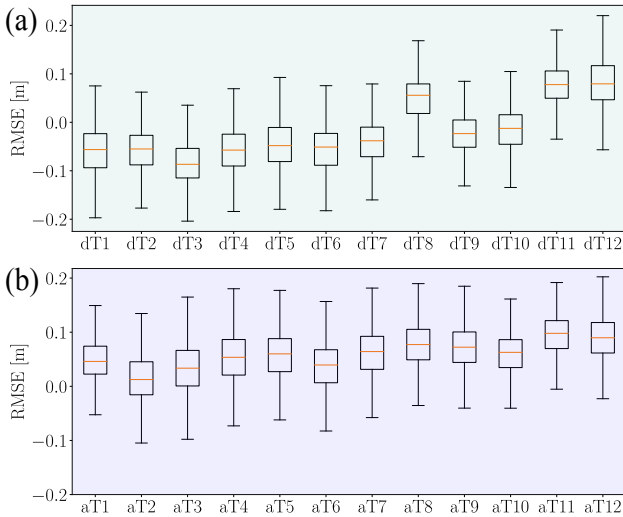


Figure 6. Measurement errors in (a) LOS distance tests and (b) LOS angle tests. We indicated the distance test and angle tests as $dT\#$ and $aT\#$, where $\#$ is the test number.

collection process. In LOS distance test, we increase the distance between anchor 1 and the tag from 0.5 meters to 6.5 meters in intervals of 0.5 meters. In LOS angle test, we change the angle between two anchors from 180° to 15° in intervals of 15° . The LOS TDOA measurement errors are summarized in Figure 6. We indicated the distance test and angle tests as $dT\#$ and $aT\#$, where $\#$ is the test number.

4.2.2 Non-line-of-sight Tests. In the NLOS identification tests, we fixed the positions of the tag and two anchors and placed different types of obstacles to create NLOS scenarios. Four reflective markers were placed on the top surface of the obstacle to indicate its position during the experiments. To reflect the comprehensive performance of UWB NLOS measurements, we selected six obstacles of different type of materials commonly used in indoor settings, including cardboard, metal, wood, plastic, and foam. Figure 7 shows the obstacles we used during the experiments.

As explained in Section 3.2, the UWB tag listens to the radio packets transmitting between anchors to compute TDOA measurements. Both NLOS conditions between one anchor and the tag and between two anchors will affect TDOA measurements. Therefore, we conducted NLOS experiments under (i) NLOS conditions between anchor 1 and the tag and (ii) NLOS conditions between anchor 1 and anchor 2 (see Figure 5c-d). Considering the different radio

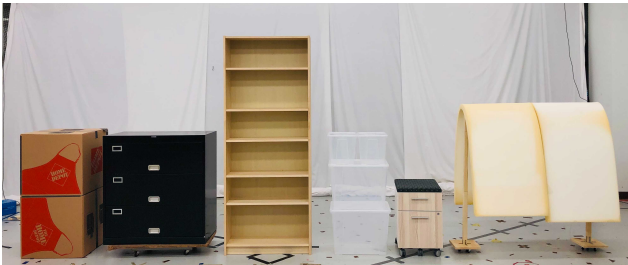


Figure 7. Obstacles used in the NLOS tests. The material of the obstacle from left to right are cardboard, metal, wood, plastic, wood, and foam.

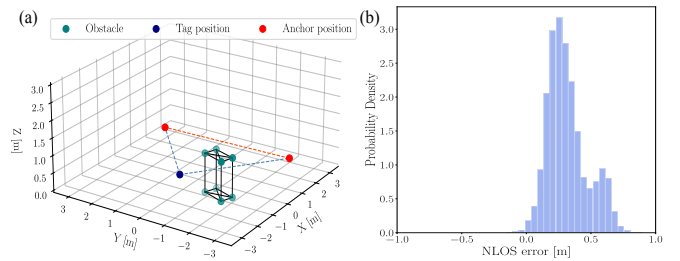


Figure 8. One example of NLOS identification experiments is shown in (a). A histogram of measurement errors induced by placing the metal obstacle between one anchor and the tag is summarized in (b).

reflection and diffraction effects with one obstacle under different orientations, we collect six sub-datasets for each NLOS condition with different orientations of the obstacle. One LOS dataset was collected for comparison. We present one NLOS identification experiment and summarize the measurement errors induced by metal occlusions in Figure 8 as an example.

4.3 Flight Dataset

The flight dataset is a comprehensive multi-modal dataset collected from a quadrotor platform in a variety of cluttered indoor environments with static and dynamic obstacles.

4.3.1 Indoor Flight Arena. We collected the UWB TDOA flight dataset in the indoor flight arena measuring approximately $7.0\text{ m} \times 8.0\text{ m} \times 3.5\text{ m}$. Printed AprilTags (Olson 2011) are attached to the soft mattresses to provide visual features for optical flow. Figure 9 is a photograph of our flight arena during data collection.

Four different anchor constellations were used for data collection. In each anchor constellation, eight UWB anchors were pre-installed in the flight arena. We refer to the Vicon frame (see Figure 9) as the inertial frame \mathcal{F}_I . Since the low-cost DWM1000 UWB chip is reported to have pose-related measurement biases (Zhao et al. 2021; Ledergerber and D’Andrea 2017), we mounted each UWB anchor to a

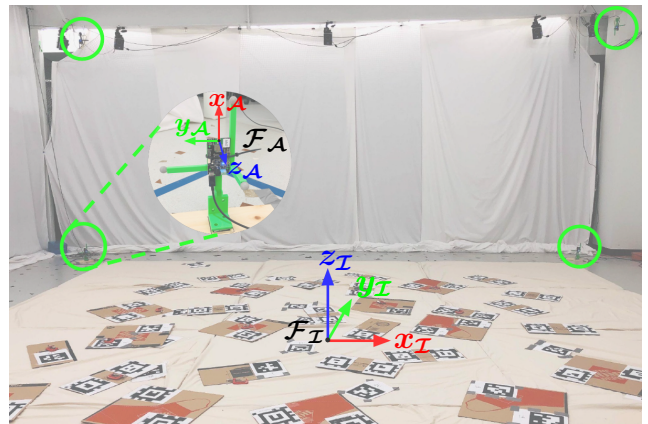


Figure 9. A photo of the flight arena. The UWB anchors are enclosed with green circles. The inertial frame and UWB anchor frame are indicated as \mathcal{F}_I and \mathcal{F}_A , respectively. The ground is covered with soft mattresses with a thickness of two inches (5.08 cm). Printed AprilTags are attached to the mattresses to provide visual features for the optical flow.

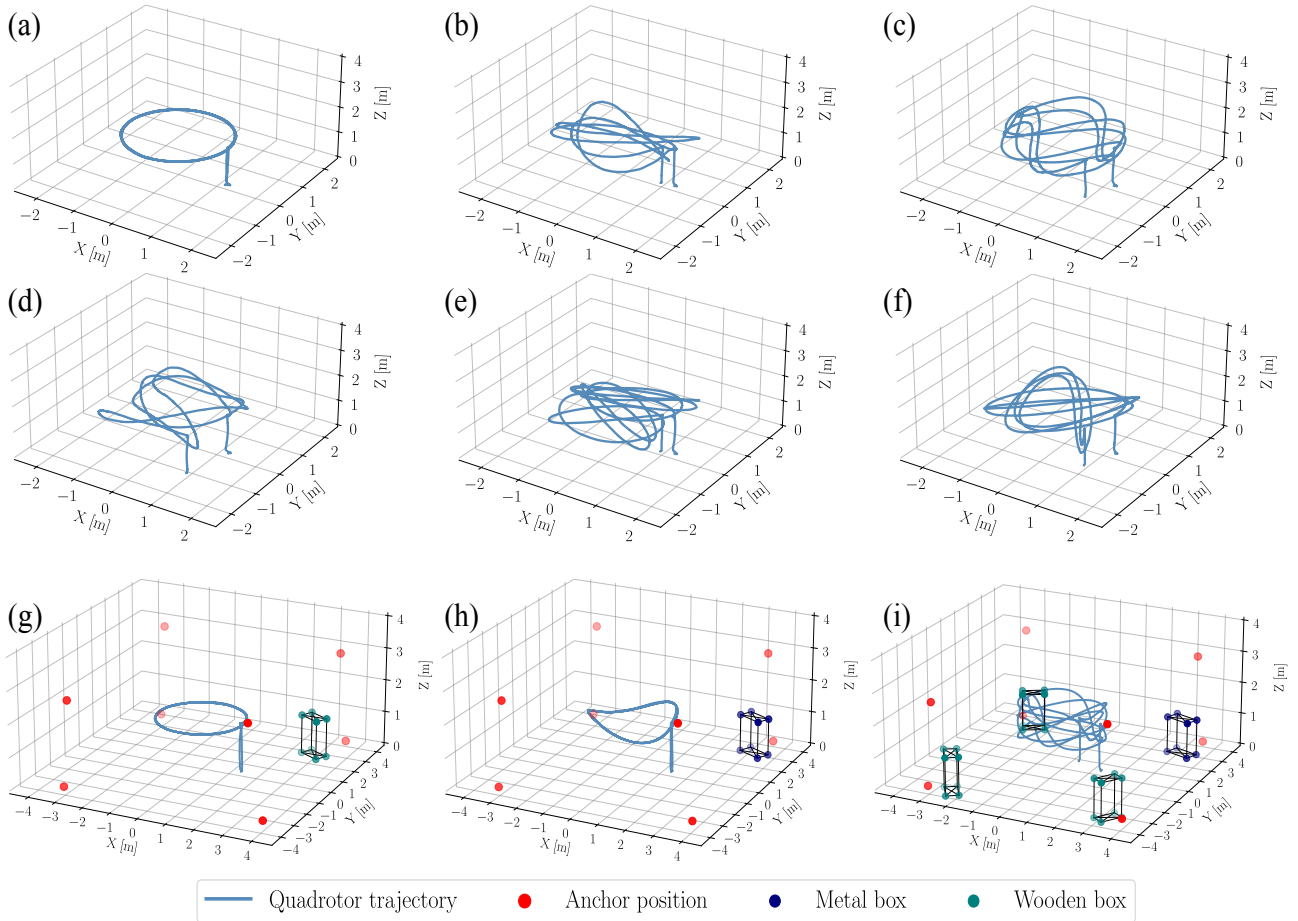


Figure 10. Flight trajectories and static NLOS conditions in the flight dataset. The six flight trajectories in constellation #1, #2, and #3 are shown in (a)-(f). Note, the trajectories in constellation #1 have a smaller separation in x and y axes due to the smaller constellation coverage. The three static NLOS conditions and the anchor positions in constellation #4 together with the three flight trajectories are shown in (g)-(i).

3D printed stand with three extended arms (see Figure 9) and used a millimeter-accurate Leica total station (Leica 2021) to survey the pose (position and orientation) of each anchor for reproducibility. We refer to the anchor frame as \mathcal{F}_A as shown in Figure 9. Note, we convert the anchor poses surveyed by the Leica total station into the inertial frame by frame alignment. To align the total station frame and the inertial frame, we used the total station to survey six reflective markers with known positions in the inertial frame and compute the transformation matrix through point cloud alignment. To assess the quality of the frame alignment between the total station frame and the inertial frame, we compute the reprojection error of the six reflective markers. The survey points in the total station frame are converted into the inertial frame with a root-mean-squared error (RMSE) of around 1.12 mm.

4.3.2 Quadrotor Platform. We built a customized quadrotor based on the Crazyflie Bolt flight controller (Bitcraze 2022a) with an inertial measurement unit (IMU) and attached commercially available extension boards (so-called decks) from Bitcraze for data collection (see Figure 11). The LPS UWB tag is mounted vertically on the top since the DWM000 antenna radiation pattern is uniform in its azimuth plane (Decaware 2016). A flow deck attached at the bottom

provides optical flow measurements and a laser-based time-of-flight (ToF) sensor provides the local altitude information. The accelerometer and gyroscope data is obtained from the onboard IMU. A micro SD card deck logs the raw sensor data received by the flight control board with high-precision microsecond timestamps. The customized quadrotor communicates with a ground station computer over a 2.4 GHz USB radio dongle (Crazyradio PA) for high-level interaction. In terms of software, we use the Crazyswarm package (Preiss et al. 2017) to send high-level commands, such as takeoff/landing and start/stop of data logging, and pre-defined waypoints. The pose of the quadrotor measured by the motion capture system is also sent to the quadrotor as an external measurement for the onboard state estimation.

4.3.3 Calibration and Latency. We refer to the offset between the center of a sensor and the center of vehicle frame \mathcal{F}_V as sensor extrinsic parameters. We calibrated the sensor extrinsic parameters by manually measuring the translation vectors from the vehicle center to onboard sensors (UWB tag and flow deck). The IMU is assumed to be aligned with the vehicle center. The translation vector from the vehicle to the UWB tag is measured as $r_{uv} = [-0.012, 0.001, 0.091]^T$ m

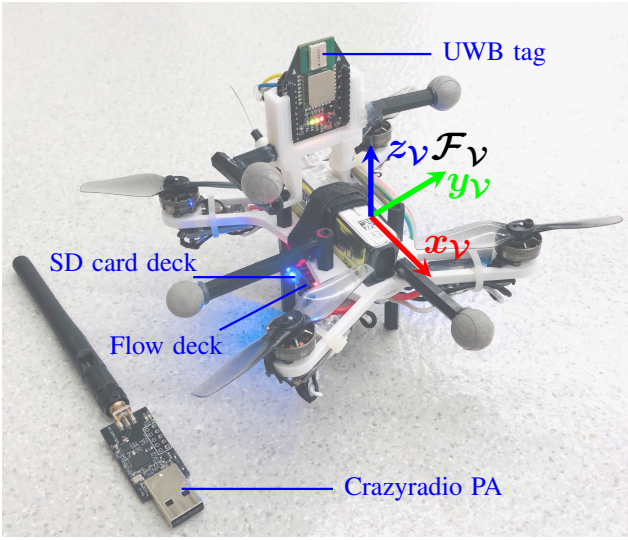


Figure 11. The customized quadrotor platform based on the Crazyflie Bolt flight controller.

and the measurement model is:

$$d_{ij} = \|(\mathbf{C}_{\mathcal{I}V}r_{uv} + \mathbf{p}) - \mathbf{a}_j\| - \|(\mathbf{C}_{\mathcal{I}V}r_{uv} + \mathbf{p}) - \mathbf{a}_i\|, \quad (4)$$

where $\mathbf{C}_{\mathcal{I}V}$ is the rotation matrix from the vehicle frame \mathcal{F}_V to the inertial frame $\mathcal{F}_{\mathcal{I}}$ and \mathbf{p} indicates the position of the vehicle expressed in the inertial frame.

Similarly, the translation vector from the vehicle to the flow-deck extension board is measured to be $r_{fv} = [0.000, 0.000, -0.012]^T$ m. Since we cover the ground of the flight arena with 2-inch thick (0.0508 m) mattresses for protection during data collection, the thickness of the mattress needs to be taken into account while using the ToF measurements. We refer to Section 6.5 of (Greiff 2017) for the detailed information of the flow-deck extension board.

We use the method provided in (Preiss et al. 2017) to measure the latency from the ground station software to the onboard firmware. We manually flicked the quadrotor and recorded the onboard microsecond timestamps where the acceleration and Vicon measurements show a corresponding spike. The offset between the two timestamps is the time delay of the radio communication between the ground station and the quadrotor. The system latency is tested to be around 10 ms.

4.3.4 Data Collection Process. We operate the motion capture system at a fixed sample frequency of 200 Hz and send the measured quadrotor pose to the onboard extended Kalman filter (EKF) with a small standard deviation, 0.001 m for position and 0.05 rad for orientation, for state estimation. Onboard the quadrotor, the raw UWB TDOA measurements, gyroscope, accelerometer, optical flow, ToF laser-ranging, barometer, and the Vicon pose measurements (sent from the ground station) are recorded as event streams. The Vicon pose measurements logged onboard are treated as the ground truth data. Each datapoint is timestamped with the onboard microsecond timer and the resulting time series are written to the micro SD card as a binary file. Python scripts are provided to parse and analyze the binary data.

We commanded the quadrotor to fly six different trajectories in constellation #1, #2 and #3 under LOS conditions.

Table 2. Format of the .csv files in each static sub-dataset.

CSV Column	Value	Description
1	d_{12} [m]	TDOA measurements $d_{12} = d_2 - d_1$
2	d_{21} [m]	TDOA measurements $d_{21} = d_1 - d_2$
3	SNR_1	SNR value of the UWB radio packet sent from anchor 1 received by the tag
4	P_{d1} [dB]	power difference value of the UWB radio packet sent from anchor 1 received by the tag
5	SNR_2	SNR value of the UWB radio packet sent from anchor 2 received by the tag
6	P_{d2} [dB]	power difference value of the UWB radio packet sent from anchor 2 received by the tag
7	SNR^{an1}	SNR value of the UWB radio packet sent from anchor 2 received by anchor 1
8	P_d^{an1} [dB]	power difference value of the UWB radio packet sent from anchor 2 received by anchor 1
9	r_{12}^{cl1} [m]	distance between anchor 1 and 2 computed by tof_{12}^{cl1}
10	SNR^{an2}	SNR value of the UWB radio packet sent from anchor 1 received by anchor 2
11	P_d^{an2} [dB]	power difference value of the UWB radio packet sent from anchor 1 received by anchor 2
12	r_{12}^{cl2} [m]	distance between anchor 1 and 2 computed by tof_{12}^{cl2}

The six flight trajectories are summarized in Figure 10a-f. In constellation #4, we created three cluttered environments with static obstacles (see Figure 10g-i) and two cluttered environments with one dynamic metal obstacle. The dynamic metal cabinet was manually moved during the flights. The onboard sensor data was collected over three different trajectories. In each experiment, we commanded the quadrotor to fly the same trajectories with both centralized and decentralized TDOA modes for comparison. For the flight experiments with dynamic obstacles, we created animations in `scripts/flight-dataset/animations` folder to demonstrate the data collection process. We also conducted a couple of manual data collections with human body involved in constellation #3 and #4.

5 Data Format

5.1 UWB Identification Data Format

The UWB identification dataset consists of data collected from (i) LOS distance and angle tests and (ii) NLOS identification experiments with different types of obstacles. In each sub-dataset, we provide a .csv file containing the collected data and a .txt file containing the poses of the tag and two anchors in one folder. For NLOS identification experiments, the positions of the four markers on the obstacles are also included in the .txt file. The format of the .csv file and brief descriptions of each value are summarized in Table 2. The format of the position

Table 3. Summary of the CSV flight dataset format.

CSV column	Name	Format
1 ~ 4	UWB TDOA	(timestamp [ms], Anchor-ID i , Anchor-ID j , d_{ij} [m])
5 ~ 8	Acceleration	(timestamp [ms], acc. x [G], acc. y [G], acc. z [G])
9 ~ 12	Gyroscope	(timestamp [ms], gyro. x [deg/s], gyro. y [deg/s], gyro. z [deg/s])
13 ~ 14	ToF laser-ranging	(timestamp [ms], ToF [m])
15 ~ 17	Optical flow	(timestamp [ms], dpixel x , dpixel y)
18 ~ 19	Barometer	(timestamp [ms], barometer [asl])
20 ~ 27	Ground truth pose	(timestamp [ms], x [m], y [m], z [m], q_x , q_y , q_z , q_w)

data provided in the .txt file is (x, y, z) in meters. The orientation is provided as a unit quaternion (q_x, q_y, q_z, q_w) , where q_w and (q_x, q_y, q_z) are the scalar and the vector components, respectively.

5.2 Flight Experiments Data Format

The flight experiment data were collected onboard the quadrotor during the flights as binary files. We provided the converted CSV and rosbag data and the corresponding Python scripts used for data parsing. For each UWB constellation, we provide the raw Leica total station survey results and computed anchor poses in .txt files. In each sub-dataset, we provide the timestamped accelerometer, gyroscope, UWB TDOA, optical flow, ToF laser-ranger, and the barometer measurements and the ground truth measurements of the quadrotor's pose during the flight. The CSV data format for each sensor data is summarized in Table 3. The detailed file structure and naming convention is shown in Figure 12.

6 Development Kit

As part of this dataset, we provided a development kit with both Python and Matlab scripts for the users to parse the data. For UWB identification dataset, we provide scripts to visualize the distribution of the collected data. For the flight dataset, we provided many different ways to visualize the sensor data and the data collection process. We also provide the STL files for the 3D printed quadrotor frame and the UWB tag support in the `setup_files/stl-files` folder. Finally, a simple extended Kalman filter (EKF) implementation is provided for users to evaluate the UWB TDOA-based positioning performance in different scenarios. The development kit and instructions can be found at <https://utiasdsl.github.io/util-uwb-dataset/>.

7 Dataset Usage

In this section, we provide two potential usages of this dataset for users.

7.1 UWB TDOA measurement modeling

For UWB TDOA localization, modeling the measurement errors under LOS and NLOS scenarios is important for the design of localization algorithms (Ruiz and Granja 2017; Prorok et al. 2012). The stationary UWB TDOA signal testing data can be used to model the distribution of the UWB TDOA measurement errors under various LOS and NLOS

conditions. One example of using the identification dataset to model UWB TDOA measurement error modeling can be found in Zhao et al. (2022).

7.2 Accurate UWB TDOA-based localization

The flight dataset can be used to develop UWB TDOA-based localization algorithms. We provide the UWB measurements under centralized TDOA mode (TDOA2) and decentralized TDOA mode (TDOA3). The flight dataset collected in constellation 1 and 2 can be used to compare the localization

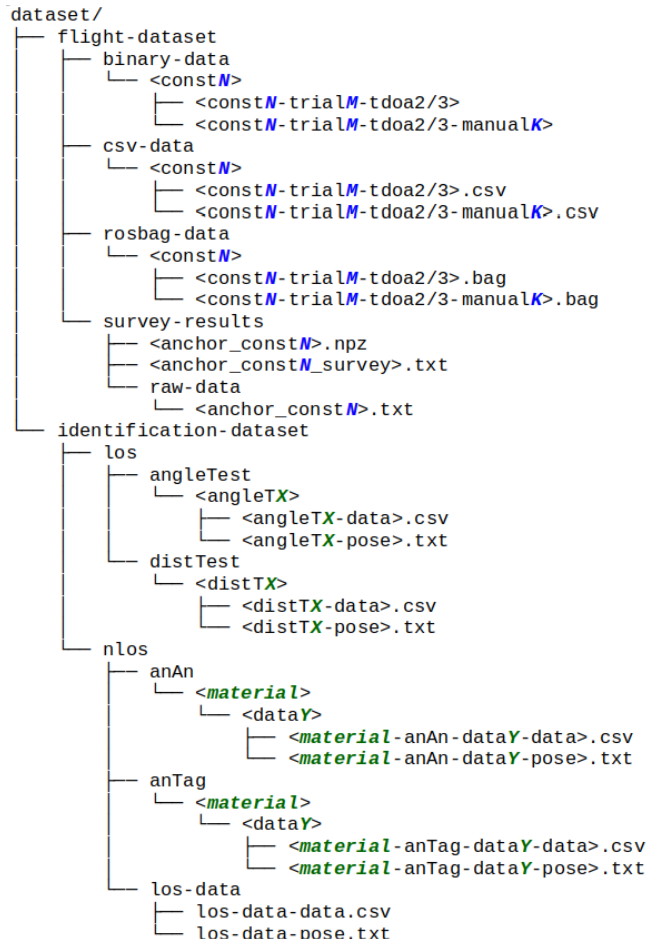


Figure 12. The file structure and naming convention of the UTIL dataset. In the flight dataset, we summarized the binary, CSV, and rosbag data according to different anchor constellations. In the identification dataset, we separate the LOS and NLOS testing data with each NLOS subdataset containing the material of the obstacle in the filename.

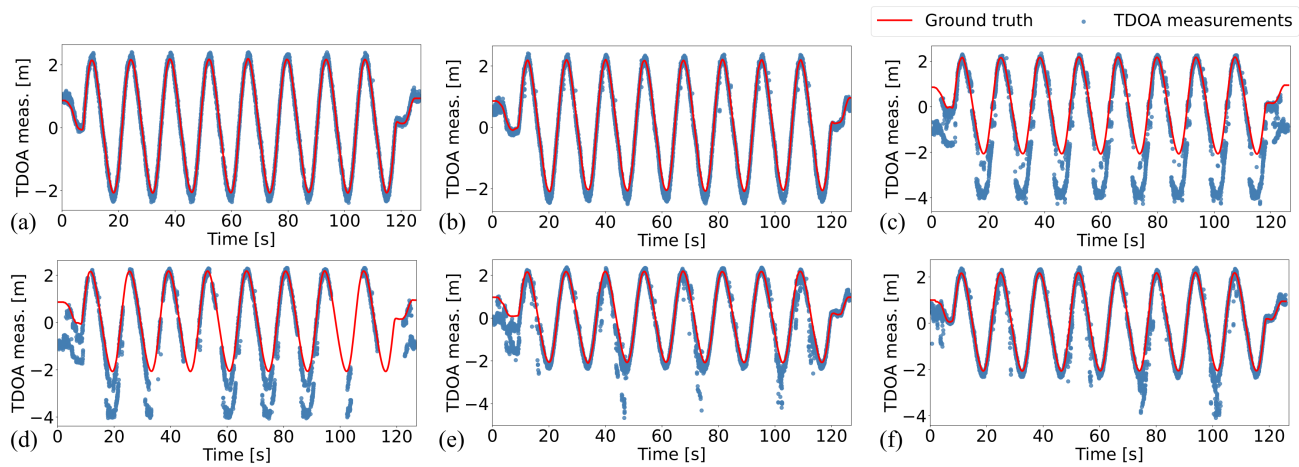


Figure 13. The UWB TDOA measurement d_{23} collected from the same circle trajectory in constellation #4 under different LOS/NLOS conditions. The measurements under clear LOS condition are shown in (a). In static NLOS conditions induced by (b) one wooden obstacle, (c) one metal obstacle, and (d) one metal and three wooden obstacles, we can observe consistent measurement biases over repeated trajectories. In dynamic NLOS conditions caused by (e) one metal obstacle and (f) one metal obstacle and three wooden obstacles, the induced measurement errors are less predictable.

performance between different UWB modes using low-cost DWM1000 UWB modules.

It is reported in the literature that the low-cost DWM1000 UWB chip suffers from systematic measurement biases (Zhao et al. 2021; Ledergerber and D’Andrea 2017). Also, the UWB radio measurements are often corrupted with multi-path and NLOS signal propagation in real-world scenarios. In cluttered indoor environments, multi-path and NLOS radio propagation cannot be avoided in general. We summarized the UWB TDOA measurement d_{23} in constellation #4 in different LOS/NLOS scenarios in Figure 13. The quadrotor was commanded to execute the same and repeated circle trajectory. We can observe in Figure 13b-d that static obstacles induce consistent influence to the UWB measurements. Also, UWB measurements can be completely blocked due to severe NLOS conditions. However, in dynamic NLOS scenarios (see Figure 13e and f), the induced measurement errors do not remain consistent. Hence, the flight dataset collected in constellation #4 can be used to design new algorithms to cope with UWB measurement errors and noise so as to achieve robust and accurate UWB-based positioning performance in such challenging and highly dynamic environments.

8 Conclusion

In this paper, we present UTIL dataset, a comprehensive UWB TDOA dataset based on the low-cost DWM1000 UWB modules. Our dataset consists of (i) an UWB identification dataset under various LOS and NLOS conditions and (ii) a multi-model flight dataset collected with a cumulative ~ 150 minutes of real-world flights in cluttered indoor environments with four anchor constellations. Obstacles of different types of materials commonly used in indoor settings, including cardboard, metal, wood, plastic, and foam, were used to create NLOS scenarios. During the flights, we collected raw UWB TDOA measurements with additional onboard sensor data (IMU, optical flow, and ToF laser) and millimeter-accurate ground truth data

from a motion capture system onboard a quadrotor platform. The combination of onboard sensors, different anchor constellations and TDOA modes, and diverse cluttered scenarios contained in this dataset enable detailed comparisons and benchmarks of UWB TDOA-based localization capabilities for quadrotors. We hope this dataset can foster research in improving the UWB TDOA-based positioning performance in cluttered indoor environments.

Acknowledgments

We would like to thank Kristoffer Richardsson and Tobias Antonsson (Bitcraze) for their guidance on the software and hardware development of the customized quadrotor platform.

References

- Adidas (2022) Adidas reveals the first fifa world cup official match ball featureing connected ball technology. URL <https://news.adidas.com/football/adidas-reveals-the-first-fifa-world-cup-official-match-ball-featuring-connected-ball-technology/s/cbb7187-a67c-4166-b57d-2b28f1d36fa0>.
- Apple (2022) Nearby interaction with UWB. URL <https://developer.apple.com/nearby-interaction/>.
- Arjmandi Z, Kang J, Park K and Sohn G (2020) Benchmark dataset of ultra-wideband radio based UAV positioning. In: *2020 IEEE 23rd International Conference on Intelligent Transportation Systems (ITSC)*. IEEE, pp. 1–8.
- Barral V, Escudero CJ, García-Naya JA and Maneiro-Catoira R (2019a) NLOS identification and mitigation using low-cost UWB devices. *Sensors* 19(16): 3464.
- Barral V, Suárez-Casal P, Escudero CJ and García-Naya JA (2019b) Multi-sensor accurate forklift location and tracking simulation in industrial indoor environments. *Electronics* 8(10): 1152.
- Bitcraze (2022a) Bitcraze Crazyflie Bolt flight controller. URL <https://www.bitcraze.io/products/crazyflie-bolt-1-1/>.

Bitcraze (2022b) Bitcraze Loco Positioning System. URL <https://www.bitcraze.io/documentation/system/positioning/loco-positioning-system/>.

Decaware (2016) Decawave DW1000 datasheet. URL <https://www.decawave.com/wp-content/uploads/2020/09/DWM1000-Datasheet.pdf>.

Decawave (2017) Decawave DW1000 user manual. URL https://www.decawave.com/sites/default/files/resources/dw1000_user_manual_2.11.pdf.

Delamare M, Duval F and Boutteau R (2020) A new dataset of people flow in an industrial site with UWB and motion capture systems. *Sensors* 20(16): 4511.

Dowsett B (2022) The world cup's new high-tech ball will change soccer forever. URL <https://fivethirtyeight.com/features/the-world-cups-new-high-tech-ball-will-change-soccer-forever/>.

Enge PK (1994) The global positioning system: Signals, measurements, and performance. *International Journal of Wireless Information Networks* 1(2): 83–105.

Ennasr O, Xing G and Tan X (2016) Distributed time-difference-of-arrival (TDOA)-based localization of a moving target. In: *2016 IEEE 55th Conference on Decision and Control (CDC)*. IEEE, pp. 2652–2658.

Greiff M (2017) *Modelling and control of the crazyflie quadrotor for aggressive and autonomous flight by optical flow driven state estimation*. Master's Thesis, Lund University.

Hamer M and D'Andrea R (2018) Self-calibrating ultra-wideband network supporting multi-robot localization. *IEEE Access* 6: 22292–22304.

KINEXON (2022) Capture and analyze the ball's position and inertial data in real-time. URL <https://kinexon.com/technology/ball-tracking/#ballsensor>.

Ledergerber A and D'Andrea R (2017) Ultra-wideband range measurement model with Gaussian processes. In: *Proc. of the IEEE Conference on Control Technology and Applications (CCTA)*. pp. 1929–1934.

Ledergerber A and D'Andrea R (2019) Ultra-wideband angle of arrival estimation based on angle-dependent antenna transfer function. *Sensors* 19(20): 4466.

Leica G (2021) Leica Geosystems Robotic Total Station. URL <https://leica-geosystems.com/products/total-stations/robotic-total-stations>.

Li J, Bi Y, Li K, Wang K, Lin F and Chen BM (2018) Accurate 3d localization for MAV swarms by UWB and IMU fusion. In: *2018 IEEE 14th International Conference on Control and Automation (ICCA)*. IEEE, pp. 100–105.

Meng W, Xie L and Xiao W (2016) Optimal TDOA sensor-pair placement with uncertainty in source location. *IEEE Transactions on Vehicular Technology* 65(11): 9260–9271.

Nguyen TH, Nguyen TM and Xie L (2021a) Range-focused fusion of camera-IMU-UWB for accurate and drift-reduced localization. *IEEE Robotics and Automation Letters* 6(2): 1678–1685.

Nguyen TM, Yuan S, Cao M, Lyu Y, Nguyen TH and Xie L (2021b) Ntu viral: A visual-inertial-ranging-lidar dataset, from an aerial vehicle viewpoint. *The International Journal of Robotics Research* : 02783649211052312.

Olson E (2011) AprilTag: A robust and flexible visual fiducial system. In: *2011 IEEE international conference on robotics and automation*. IEEE, pp. 3400–3407.

Pfeiffer S, De Wagter C and De Croon GC (2021) A computationally efficient moving horizon estimator for ultra-wideband localization on small quadrotors. *IEEE Robotics and Automation Letters* 6(4): 6725–6732.

Preiss JA, Honig W, Sukhatme GS and Ayanian N (2017) Crazyswarm: A large nano-quadcopter swarm. In: *2017 IEEE International Conference on Robotics and Automation (ICRA)*. IEEE, pp. 3299–3304.

Prorok A, Gonon L and Martinoli A (2012) Online model estimation of ultra-wideband TDOA measurements for mobile robot localization. In: *2012 IEEE International Conference on Robotics and Automation*. Ieee, pp. 807–814.

Qorvo (2022) Qorvo UWB solutions certified for Apple U1 interoperability. URL <https://www.qorvo.com/newsroom/news/2022/qorvo-uwb-solutions-certified-for-apple-u1-interoperability>.

Queraltà JP, Almansa CM, Schiano F, Floreano D and Westerlund T (2020) UWB-based system for UAV localization in GNSS-denied environments: Characterization and dataset. In: *2020 IEEE/RSJ International Conference on Intelligent Robots and Systems (IROS)*. IEEE, pp. 4521–4528.

Raza U, Khan A, Kou R, Farnham T, Premalal T, Stanoev A and Thompson W (2019) Dataset: Indoor localization with narrow-band, ultra-wideband, and motion capture systems. In: *Proceedings of the 2nd Workshop on Data Acquisition to Analysis*. pp. 34–36.

Robert Triggs CW (2022) What is UWB, and why is it in my phone? Ultra-wideband technology, explained. URL <https://www.androidauthority.com/what-is-uwb-1151744/>.

Ruiz ARJ and Granja FS (2017) Comparing Ubisense, Bespoon, and Decawave UWB location systems: Indoor performance analysis. *IEEE Transactions on instrumentation and Measurement* 66(8): 2106–2117.

TDSR (2022) TDSR P440 time domain UWB module. URL <http://tdsr-uwb.com/products-p440-uwb-module/>.

Vicon MCS (2022) Vicon Vantage+ cameras. URL <https://www.vicon.com/hardware/cameras/vantage/>.

Vleugels R, Van Herbruggen B, Fontaine J and De Poorter E (2021) Ultra-wideband indoor positioning and IMU-based activity recognition for ice hockey analytics. *Sensors* 21(14): 4650.

Zafari F, Gkelias A and Leung KK (2019) A survey of indoor localization systems and technologies. *IEEE Communications Surveys & Tutorials* 21(3): 2568–2599.

Zhao W, Goudar A and Schoellig AP (2022) Finding the right place: Sensor placement for UWB time difference of arrival localization in cluttered indoor environments. *IEEE Robotics and Automation Letters* .

Zhao W, Panerati J and Schoellig AP (2021) Learning-based bias correction for time difference of arrival ultra-wideband localization of resource-constrained mobile robots. *IEEE Robotics and Automation Letters* 6(2): 3639–3646.

Zhengliang Z, Degui Y, Junchao Z and Feng T (2021) Dataset of human motion status using IR-UWB through-wall radar. *Journal of Systems Engineering and Electronics* 32(5): 1083–1096.